A probabilistic assessment of geomechanical reservoir integrity during CO₂ sequestration in flood basalt formations

Richard S. Jayne (iD), **Hao Wu** (iD) **and Ryan M. Pollyea** (iD), Department of Geosciences, Virginia Polytechnic Institute & State University, Blacksburg, VA, USA

Abstract: Recent field experiments in Iceland and Washington State (USA) show that basalt formations may be favorable targets for carbon capture and sequestration (CCS) because CO_2 mineralization reactions proceed rapidly. These results imply that there is tremendous opportunity for implementing CCS in large igneous provinces. However, the magnitude of this opportunity comprises commensurate levels of uncertainty because basalt reservoirs are characterized by highly heterogeneous, fracture-controlled hydraulic properties. This geologic uncertainty is propagated as parametric uncertainty in quantitative risk models, thus limiting the efficacy of models to predict CCS performance attributes, such as reservoir integrity and storage potential. To overcome these limitations, this study presents a stochastic approach for quantifying the geomechanical performance attributes of CCS operations in a highly heterogeneous basalt reservoir. We utilize geostatistical reservoir characterization to develop an ensemble of equally probable permeability distributions in a flood basalt reservoir with characteristics of the Wallula Basalt Pilot Project. We then simulate industrial-scale CO_2 injections within the ensemble and calculate the mean and variance of fluid pressure over a 1-year injection period. These calculations are combined with the state of stress in southeast Washington State to constrain the spatial extent at which shear failure, fracture initiation, and borehole breakdown may occur. Results from this study show that (i) permeability uncertainty alone causes injection pressure to vary over 25 MPa, (ii) shear failure is likely to occur at 7 times greater distances from the injection than the CO_2 migrates, and (iii) joint initiation pressures are localized within the volume comprising the CO_2 plume. © 2019 Society of Chemical Industry and John Wiley & Sons, Ltd.

Keywords: numerical modeling; permeability; heterogeneity; CO_2 sequestration; Columbia River Basalt Group

Introduction

A growing body of evidence suggests that deep basalt reservoirs (>800 m) may be attractive targets for carbon capture and sequestration (CCS) on the basis of favorable CO_2–water–rock reaction kinetics, which result in permanent CO_2 isolation through mineral trapping.[1,2] Recent pilot-scale experiments have provided evidence of *in situ* mineralization of the injected CO_2 within basalt

SCI

reservoirs. The CarbFix CCS pilot in Iceland injected 230 tons of CO$_2$ dissolved in water into a basalt reservoir, and postinjection analysis showed 95% of the CO$_2$ was permanently converted to mineral phases just 2 years after injection.[3] The Wallula Basalt Sequestration Pilot Project in eastern Washington injected 1000 metric tons (MT) of supercritical CO$_2$ into the Columbia River Basalt Group (CRBG) and postinjection analysis showed that carbonate nodules in sidewall cores were (i) widespread and (ii) composed of the same isotope signature as the injected CO$_2$.[4] To complement these results, CCS in deep basalt reservoirs is motivated to a large extent by the relatively high storage potential within both onshore and offshore basalt formations. In particular, CO$_2$ storage estimates for the Columbia River Basalt Group in the northwestern United States are estimated to be on the order of 100 Gt CO$_2$,[1] and offshore basalt formations within the Juan de Fuca plate and Central Atlantic Magmatic Province hold potential for CO$_2$ disposal on comparable scales.[5,6] However, the injection of CO$_2$ into the subsurface causes a disturbance in the pressure, temperature, and chemical systems within the target reservoir, and this response affects the injectivity, storativity, and confinement potential of the site. While the Wallula Pilot Borehole and CarbFix projects show promising results, transitioning basalt CCS technology from pilot scale to industrial applications is complicated by the highly heterogeneous nature of fracture-controlled basalt reservoirs.[7]

Among the principal challenges for industrial-scale CCS in any geologic environment is to ensure >99% CO$_2$ isolation per thousand years,[8] which, if not met, will likely postpone rather than mitigate global warming trends.[9] In order to achieve >99% CO$_2$ isolation, the integrity of physical traps (i.e., cap-rock seals) under long-term injection pressure is a paramount concern because excessive reservoir pressure may result in a number of adverse consequences, including fracture propagation/reactivation,[10,11] shear or joint dilation,[12] induced seismicity,[13] and cm-scale displacements on small, difficult to characterize faults and fractures.[14] As a result, geomechanical reservoir integrity has become an important criterion for numerical model-based risk assessment in CCS reservoir siting.[15] In order to address this problem, stochastic methods have been increasingly deployed to understand how spatial, parametric, and geologic uncertainty affects CCS reservoir performance.[16–22] For example, Pollyea

et al.[19] develop and implement ensemble simulation methods to quantify spatially variable sealing behavior within the low-volume Snake River Plains basalts. Jayne *et al.*[23] extend these methods into flood basalt formations to show how permeability uncertainty affects the injectivity and leakage during CCS in flood basalt formations. And in sedimentary basins, Bosshard *et al.*[24] show that heterogeneous properties in a sandstone reservoir impose significant controls on both CO$_2$ injection rate and storage capacity.

Stochastic simulation methods have been gaining traction as a way to bound the uncertainties associated with heterogeneous reservoirs because spatially variable properties, such as permeability, cannot be upscaled according to simple averaging rules.[25] It is the uncertainty of permeability distribution at these larger scales that can have a substantial impact on the results of hydrogeologic models.[18,19] For example, constraining permeability at regional scales has implications for studying geological formations that contain multiple resources (e.g., groundwater, geothermal, and carbon storage).[26] Complete characterization of the geomechanical response to deep CO$_2$ injections requires *a priori* knowledge of regional tectonic stresses, mechanical reservoir properties, and orientations of preexisting discontinuities (faults and fractures) within the reservoir. Within CRBG reservoirs, pressure build up is a particular concern because both reservoir and seal rock are ubiquitously fractured. Furthermore, pressure builds rapidly in early time during a CO$_2$ injection. Mathias *et al.*[27] and Pollyea[28] illustrate that the majority of fluid pressure accumulation occurs within the first few days of a CO$_2$ injection. This rapid pressure build up in early time is critically important to account for when studying the geomechanical response of the storage reservoir. In order to assess how reservoir integrity is affected by rapid pressure accumulation and heterogeneous reservoir properties, this study utilizes a Monte Carlo modeling approach to simulate a CCS injection scenario into the Columbia River Basalt Group. Specifically, we use ensemble simulation methods in combination with known geologic information from the Wallula borehole to quantify how permeability variability affects reservoir integrity during an industrial-scale CO$_2$ injection. Ensemble analytics are utilized to develop a probabilistic assessment of geomechanical reservoir integrity during CCS operations in a flood basalt reservoir with characteristics of the Wallula Basalt Sequestration Pilot Project.
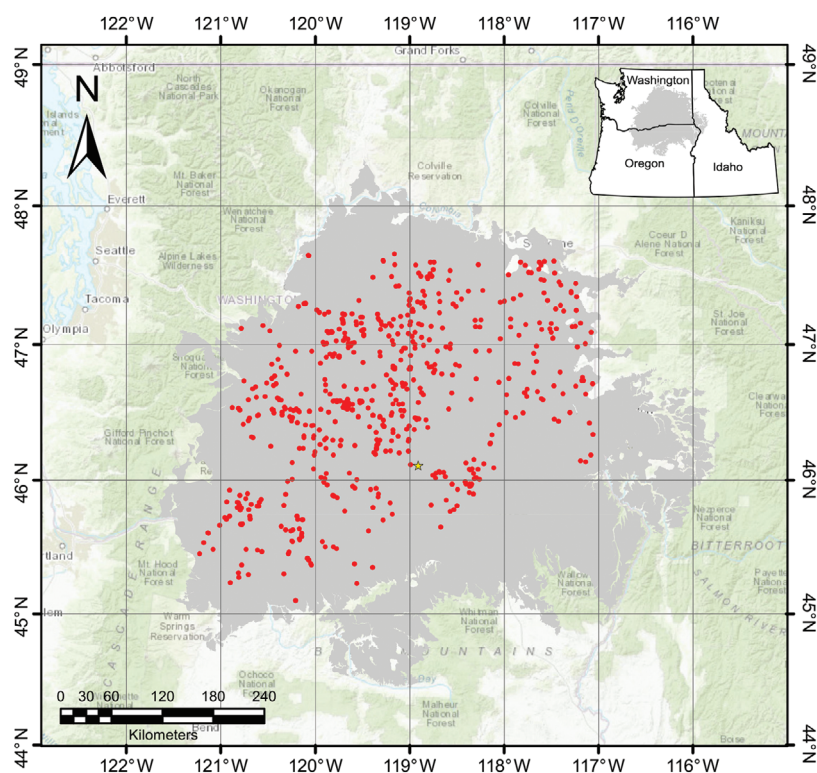
Figure 1. Map showing the areal extent of the Columbia River Basalts shaded in gray. Wells with permeability data compiled by Jayne and Pollyea[36] within the CRBG are shown in red and the Wallula pilot borehole is denoted by the yellow star (modified from Jayne and Pollyea[36]).

Geologic setting

Columbia river basalt group

The CRBG is a continental large igneous province in the northwest United States (Fig. 1), and comprises a layered assemblage of ~300 Miocene-age flood basalts with an areal extent of 200 000 km^2, aggregate thickness of 1–5 km, and total estimated volume of 224 000 km^3.[29,30] The CRBG has been extensively studied due to its wide range of resource potential, including (1) groundwater production,[31,32] (2) nuclear waste storage,[33] (3) natural gas storage,[29] (4) geologic CO$_2$ sequestration,[4] and (5) geothermal resources.[34] Among the principal challenges in assessing the feasibility of engineered CRBG reservoirs is to understand how fracture-controlled reservoir properties (i.e., permeability and porosity) affect both local- and regional-scale fluid flow. These fracture-controlled reservoir properties are governed by individual basalt flow morphology, which is characterized by (1) densely fractured, vesicular flow-tops, (2) a central entablature comprising narrow, fanning columnar joints, and (3) lower colonnades with vertical, column bounding joints (Fig. 2).[35] Within CRBG flows, *in situ* pumping tests reveal that permeability ranges over 13 orders of magnitude with the entablature zone generally inhibiting groundwater flow (Fig. 3A), while densely fractured flow tops and flow bottoms are highly productive.[32,36] To further complicate CRBG reservoir characterization, individual basalt flows exhibit km-scale lateral dimensions and vertical dimensions from centimeter scale to more than 70 m.[35]

Wallula pilot borehole

As part of the Big Sky Carbon Sequestration Partnership (BSCSP), U.S. Department of Energy identified the CRBG as a primary target formation for CCS development in the Pacific Northwest. The CRBG was chosen on the basis of its relatively high CO$_2$ storage estimates (10–50 Gt CO$_2$), potential for CO$_2$ isolation, and generally favorable reservoir characteristics.[1,4,37,38] In order to locate a suitable site for a pilot injection, seismic surveys were conducted in Walla Walla County, WA, which identified areas where
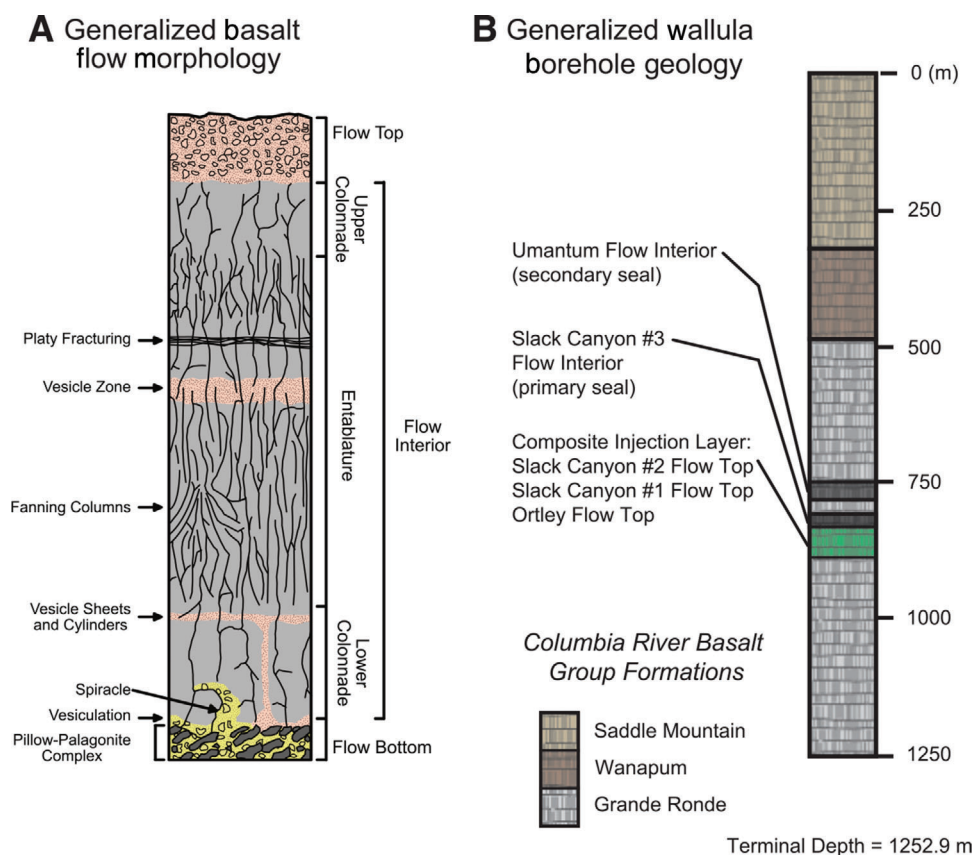
Figure 2. (A) Individual CRBG flow morphology (modified from Reidel *et al.*[29]).
(B) Generalized geology within the Wallula pilot borehole.

major geologic structures would not preclude a CO_2 injection.[39] Drilling for the Wallula Pilot Borehole began in January 2009 and completed in April 2009. The Wallula Pilot Borehole reaches a total depth of 1253 m and intersects three CRBG formations: Saddle Mountain, Wanapum, and Grande Ronde.[30] The target formation for injection is the Grande Ronde Basalt, of which the Wallula Pilot Borehole intersects 26 flows and 7 members. A candidate (composite) injection zone was identified at 828– 887 m depth, spanning three brecciated interflow zones within the Grande Ronde Formation.[30] Hydrologic characterization of these three zones shows that they represent a single hydraulic unit with relatively high permeability and are bounded by thick low permeability flow interiors, which act as a natural caprock.[30] In 2013, 1000 MT of supercritical CO_2 was injected at the Wallula Pilot Borehole over the course of 3 weeks. Since the injection, McGrail *et al.*[4] have published results from this field study validating the reactivity of supercritical CO_2 with basalts at the Wallula Pilot Borehole.

Methods

This study uses numerical modeling and simulation to test the feasibility of industrial-scale CO_2 injections at the Wallula Basalt Sequestration Pilot Site in southeast Washington State (USA). The model scenario reproduces known hydraulic properties within the Wallula borehole, but far-field permeability distributions are subject to substantial uncertainty. To bound this uncertainty, an ensemble of equally probable synthetic reservoirs is developed on the basis of geostatistical reservoir simulation.[40] The model scenario simulates CO_2 injections for 1 year within each synthetic reservoir, and the complete set is analyzed using ensemble simulation methods. This results in a probabilistic model of CO_2 transport and injection-induced pressure transients. This probabilistic model is the basis for calculating geomechanical reservoir integrity using static threshold criteria calculated along with utilizing the variance associated with the ensemble simulation methods to account for 3σ variability.
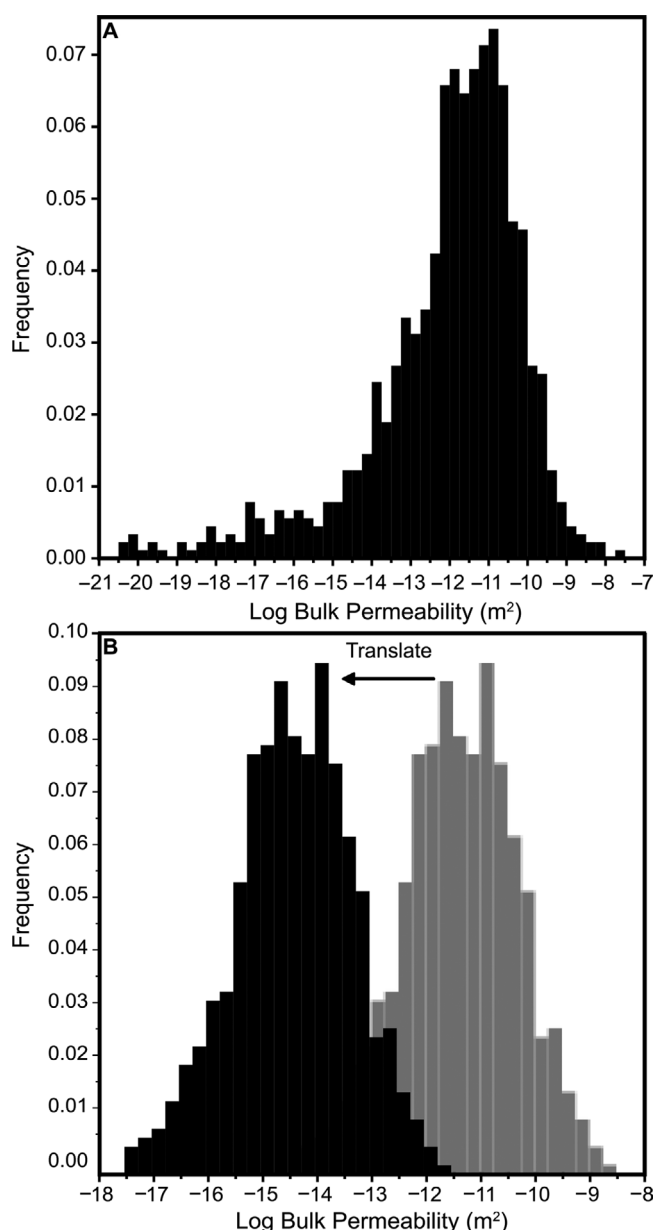
Figure 3. (A) Histogram of log permeability from well data compiled by Jayne and Pollyea[36]. (B) Histogram of the filtered permeability data to represent the high permeability flow tops. The mean of log permeability is −11.5 m^2 (gray) in order to make this range of permeabilities more representative; at the depth of the injection zone, the permeability distribution is translated downward so that the mean log permeability is −14.5 m^2, which is congruent with field test from the Wallula borehole.

Reservoir characterization and model domain

The conceptual model is based on geologic characteristics of the Wallula Basalt Sequestration Pilot

site, which is a layered assemblage of individual basalt flows with alternating high permeability flow tops/bottoms and low permeability flow interiors (Fig. 4). The Wallula injection zone occurs between 775 and 865 m depth, within which permeability is well constrained on the basis of highly detailed site characterization.[30] Nevertheless, permeability beyond the borehole is both highly heterogeneous and highly uncertain due to the fracture-controlled nature of basalt formations.[36] To account for this uncertainty in numerical simulation, this study implements stochastic reservoir characterization to develop an ensemble of 35 equally probable reservoir domains that each reproduce known borehole geology, but model far-field permeability on the basis of (i) the semivariogram correlation structure of CRBG permeability and (ii) its corresponding probability distribution.

The spatial correlation of CRBG permeability was shown by Jayne and Pollyea[36] to exhibit spatial anisotropy with directions of maximum and minimum spatial correlation oriented at N40°E and N130°E, respectively. This spatial correlation model is based on a regional CRBG permeability database (Fig. 1) for which permeability values were filtered on two standard deviations of the mean to ensure that the low permeability entablature (caprock) was not incorporated in the calculations and only the highly productive flow tops and bottoms were included (Fig. 3B). The present study adopts this convention to constrain permeability distribution within the highly conductive composite injection zone. This results in a range of log permeability (log k) from −8.5 m^2 to −14.5 m^2 with a median log k of −11.5 m^2. However, the present study is focused on permeability at depths greater than 750 m, where the log k in the Wallula Pilot Borehole is known to be approximately −14.5 m^2.[30] This discrepancy arises because the vast majority of permeability measurements in the Jayne and Pollyea's[36] database are taken at depths less than ∼200 m; however, CRBG permeability decreases with depth until ∼1000 m. To account for this difference, we adopt the method proposed by Gierzynski and Pollyea[21] that translates the distribution such that the variability of permeability is maintained but the mean permeability is representative of the composite injection in the Wallula Pilot Borehole. This results in a new range of log k from −11 to −17 m^2. This probability distribution is combined with the anisotropic semivariogram model to develop 35 equally probable realizations of the composite injection zone by
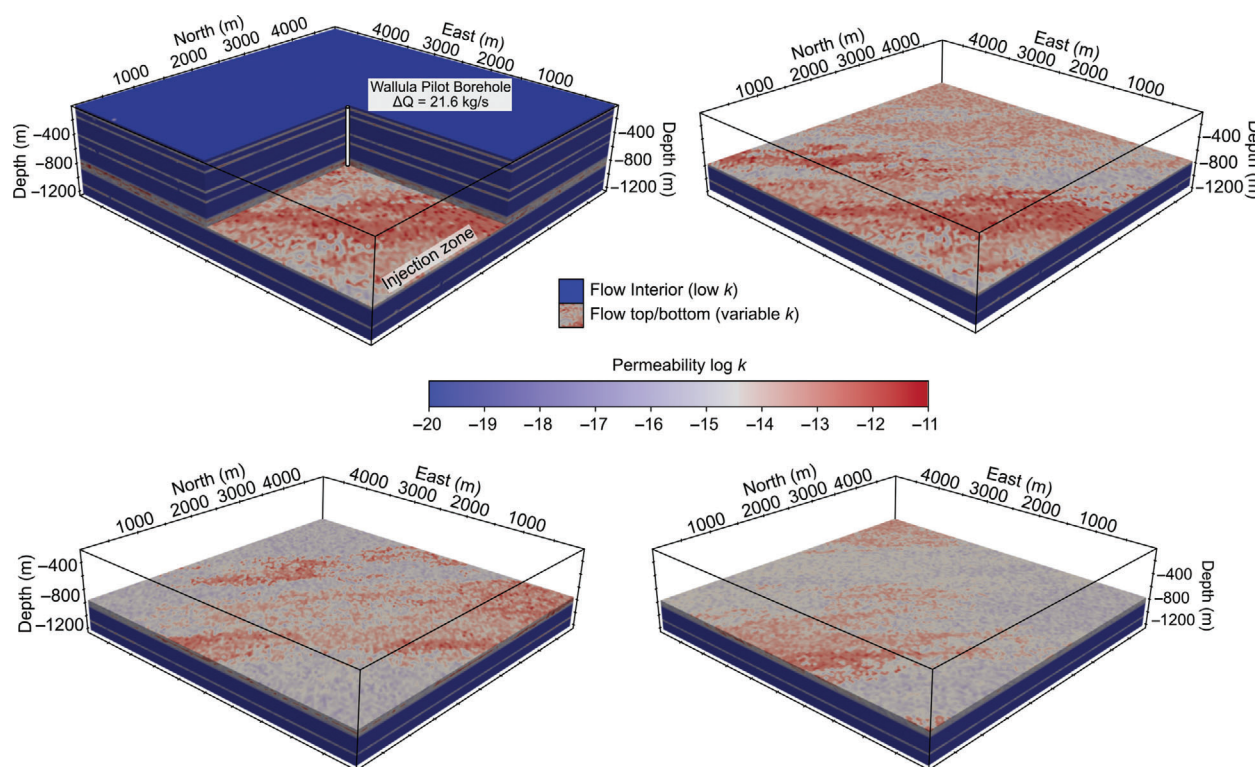
Figure 4. Model domain for CO$_2$ injection modeling study. The composite injection zone is between 775 and 865 m depth and is populated with spatially correlated, randomly generated permeability distributions. The cut-away shows the alternating layers of flow interior and flow tops along with the location of the Wallula pilot borehole. Three spatially correlated and equally probable permeability distributions are shown in the other panels.

sequential indicator simulation.[41] In this approach, each grid cell is simulated in random order by solving the ordinary kriging equations on the basis of (1) the cumulative distribution function for CRBG permeability, (2) known data points, which are the borehole permeability tests from the Wallula borehole, (3) previously simulated grid cells, and (4) the chosen spatial correlation model, which for this study is the anisotropic semivariogram model developed Jayne and Pollyea.[36] For this study, the permeability distribution is simulated for 35 equally probable composite injection zones, each of which reproduces known borehole permeability, as well as the depth-scaled CRBG permeability distribution and spatial correlation characteristics with minor ergotic fluctuation.

Each composite injection zone permeability distribution is inserted into the overall model domain, which comprises an areal extent of 5000 m × 5000 m × 1250 m representing the ground surface to 1250 m depth with the Wallula Pilot Borehole centrally located. Individual grid blocks have a maximum dimension of 50 m × 50 m × 25 m in the far-field with higher

resolution grid refinement of 5 m × 5 m × 5 m near the injection well (Fig. 4). The complete domain is discretized into 1 467 568 grid blocks by Voronoi tesselation.[42] A total of 35 individual model domains are produced with spatially variable and equally probable permeability distributions in the composite injection zone.

Numerical simulation

In this study, CO$_2$ injection is simulated within each equally probable synthetic reservoir for 1 year at 21.6 kg/s, which corresponds with the typical CO$_2$ output from a 500 MW gas-fired power plant. The code selection for this study is TOUGH3[43] compiled with the ECO2M fluid property module.[44] TOUGH3 solves energy and mass conservation equations for nonisothermal, multiphase flows in a porous geologic media. The ECO2M module simulates mixtures of H$_2$O–NaCl–CO$_2$, within the temperature range of 10–110°C, pressure ≤60 MPa, and salinity from nil to full halite saturation. The ECO2M module simulates all

 |

Table 1. Model parameters.

	Matrix	Fracture	Flow top	Basal boundary
Density (kg·m^{-3})	2900.0	2300.0	2300.0	2900.0
Porosity	0.05	0.1	0.3	0.05
Permeability (m^2)	10^{-20}	10^{-16}	Varies	10^{-20}
Thermal conductivity (W·m°C^{-1})	2.11	2.11	2.11	2.11
Heat capacity (J·kg^{-1}°C^{-1})	840	840	840	840

van Genuchten parameters				
Relative permeability		Capillary pressure		
λ	0.550	λ		0.457
S_{lr}	0.30	S_{lr}		0.0
S_{ls}	1.0	α (Pa^{-1})		5.e-5
S_{gr}	0.25	P_{max} (Pa)		1e.7
		S_{ls}		0.999

possible phase conditions for CO$_2$–brine mixtures, including transitions between super- and subcritical CO$_2$, as well as the transition between liquid and vapor CO$_2$.[44]

Initial conditions are specified with a hydrostatic pressure gradient ranging from 0.101 MPa (1 atm) at ground surface to 12.3 MPa at the bottom of the Wallula Pilot Borehole. Initial temperature is calculated by imposing the regional heat flux of ~65 mW/m^2 [45] as a thermal boundary at the base of the model and a constant temperature of 10°C at ground surface. This results in a linear temperature gradient from 10°C at the surface to 50°C at 1250 m depth. The reservoir water within the CRBG is defined by a NaCl concentration of 10 000 ppm. These initial conditions are consistent with the field measurements taken at the Wallula Pilot Borehole.[30] Within the composite injection zone (775–865 m), initial temperature and pressure conditions range from 35 to 38°C and 7.7 to 8.4 MPa, which are within the supercritical field for CO$_2$. Dirichlet boundary conditions are specified at (i) the upper boundary of the model domain to hold pressure and temperature constant at ground surface and (ii) the lateral boundaries of the model domain to maintain temperature and pressure gradients in the far field.

For this modeling study, the relative permeability, capillary pressure models, and geologic properties are listed in Table 1. The bulk reservoir properties for the CRBG are based on petrophysical[46] and modeling[21] studies extant in the literature. The effects of

multiphase flow (CO$_2$ and brine) are accounted for using the van Genuchten[47] models for relative permeability and capillary pressure (Table 1). It is important to note here that relative permeability of basalt flows remains a subject of much uncertainty[28]; however, it is generally accepted that the relative permeability characteristics of basalt fractures are highly interfering Bertels *et al.*[48]

As with all modeling studies, a brief mention of the model limitations is warranted. This modeling study does not account for basalt dissolution or secondary mineral precipitation, so permeability alteration from secondary mineral precipitation is neglected. Thus, the simulation results presented here are a conservative estimate of both CO$_2$ storage potential and fluid pressure accumulation. In addition, relative permeability hysteresis is not accounted for in the simulations because only the injection phase of a CCS project is simulated, thus imbibition does not occur. Similarly, mass transport by molecular diffusion is not accounted for because CO$_2$ is under constant injection pressure, which results in a high Péclet number. And finally, geomechanical reservoir integrity is evaluated on the basis of threshold criteria that depend on changes in fluid pressure, thus geomechanical *processes* are not explicitly simulated.

Data analysis

The simulations that completed each discrete time step were analyzed using ensemble simulation analytics

Table 2. Geomechanical parameters.

μ_s	0.85	50
T_o (MPa)	1.5	72
β_i (MPa^{-1})	1.9×10^{-11}	72
β_b (MPa^{-1})	4.8×10^{-11}	72
K_{IC} (MPa m$^{\frac{1}{2}}$)	2.203	51
Y	$\frac{2}{\sqrt{\pi}}$	51
c (mm)	0.01	63
ν	0.3	72

(e-type estimates).[41] In this approach, the mean and variance of fluid pressure and free-phase CO$_2$ saturation are calculated for each grid cell. The e-type calculation for mean fluid pressure ($\bar{P}_{f,(x,y,z)}$) within each grid cell is

$$\bar{P}_{f(x,y,z)} = \frac{1}{35} \sum_{i=1}^{35} P_{f,i(x,y,z)} \qquad (1)$$

where, $P_{f,i(x,y,z)}$ is the modeled fluid pressure for simulation i at location (x, y, z). Similarly, the variance ($s^2_{(x,y,z)}$) associated with Eqn (1) for each grid cell is computed as:

$$s^2_{(x,y,z)} = \frac{1}{35} \sum_{i=1}^{35} (P_{f,i(x,y,z)} - \bar{P}_{f,(x,y,z)})^2 \qquad (2)$$

Because reservoir integrity during CCS is based to a large extent on injection-induced fluid pressure transients, the ensemble analysis (Eqns (1) and (2)) forms the basis for calculating geomechanical threshold criteria with corresponding uncertainty estimates. The geomechanical parameters used to calculate these threshold criteria can be found in Table 2. However, these calculations require knowledge about the regional stress state within the CRBG in southeast Washington. Stress data are available from site characterization efforts at the Hanford Nuclear Reservation, which is located ~30 km northeast of the Wallula site. Specifically, *in situ* stress measurements are reported from borehole tests between 924 and 1195 m depth,[49] which is ~40 m below the Wallula composite injection zone and show that the CRBG are within a compressive regime where the minimum compressive stress is vertical (Fig. 5). Extending a linear regression model of S$_H$ and S$_V$ to 800 m depth suggests 38 MPa differential stress within the CO$_2$ injection zone (Fig. 5). These are combined with a
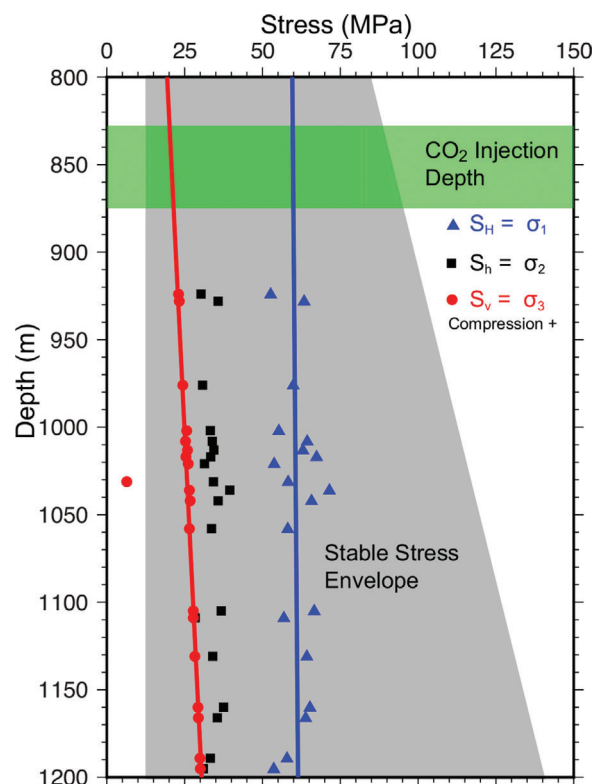

Figure 5. Regional stress state near the Wallula Basalt Sequestration Pilot Project. Maximum compressive horizontal stress (S$_H$), minimum compressive horizontal stress (S$_h$), and lithostatic stress (S$_V$) are *in situ* stress measurements at Hanford Nuclear Reservation, approximately 60 km northwest of the Wallula site. Gray Shading denotes a stable stress field on the basis of Mohr–Coloumb failure criteria. Green shading denotes the depth interval for CO$_2$ injection at the Wallula site (modified from Pollyea[28]).

friction coefficient (μ_s) of 0.85[50] to estimate the upper and lower bounds of stable stress as

$$\sigma_1 = \sigma_3 [(\mu_s^2 + 1)^{1/2} + \mu_s]^2 \qquad (3)$$

$$\sigma_3 = \sigma_1 [(\mu_s^2 + 1)^{1/2} + \mu_s]^{-2} \qquad (4)$$

where σ_1 and σ_3 are the maximum and minimum compressive stresses, respectively.[51] Equations (3) and (4) assume that internal cohesion is nil because fractures are weaker than intact rock and mounting pore fluid pressure will significantly reduce fault and/or fracture cohesion.[51]

Since the disposal reservoir is fully saturated, effective stress theory is invoked to account for the influence of pore fluid pressure acting in opposition to the compressive stresses, for example, S$_{V,eff}$ = S$_V$ − P$_f$. In

|

the context of Fig. 5, pore fluid pressure translates S_H, S_h, and S_V to the left, while the failure criteria exhibit a nonlinear translation such that the upper bounding failure line is reduced in greater proportion than the minimum bound.[51] This means that the envelope of stable stress narrows while differential stress remains unchanged, so that $S_{V,eff}$ becomes closer to the minimum bounding failure line. To quantify which CO$_2$ injection scenarios produce sufficient pore fluid pressure to move $S_{V,eff}$ out of the stable stress envelope, the Mohr–Coulomb failure criteria is evaluated within each grid cell of the simulation ensemble by calculating the mean minimum effective compressive stress ($\bar{S}_{V,eff(x,y,z)}(t)$) within each grid cell of the model domain as

$$\bar{S}_{V,eff(x,y,z)}(t) = S_V - \bar{P}_{f(x,y,z)}(t) \qquad (5)$$

Here, S_V is the vertical stress (σ_3) and $\bar{P}_{f(x,y,z)}(t)$ is mean grid block injection pressure for time step (t) computed as per Eqn (1). Once all $\bar{S}_{V,eff(x,y,z)}(t)$ are computed for each CO$_2$ injection scenario, the likelihood of failure less than 1% for each grid cell is computed as

$$\text{Failure} \ > 1\% \ \text{if}: \bar{S}_{V,eff(x,y,z)}(t) - 3s_{(x,y,z)}$$
$$> S_H[(\mu_s^2 + 1)^{1/2} + \mu_s]^2 \qquad (6)$$

where $S_H[(\mu_s^2 + 1)^{1/2} + \mu_s]^{-2}$ is the lower bound of σ_3 given in Eqn (4), and $s_{(x,y,z)}$ is the standard deviation of mean grid cell pore fluid pressure (square root of Eqn (2)).

Increasing fluid pressure during CO$_2$ injections may result in fracture dilation and fracture propagation, both of which can occur at scales ranging from local borehole effects to far-field reservoir effects. Within CRBG reservoirs, fracture dilation is a particular concern because densely fractured entablature zones represent the cap rock seal for CO$_2$ isolation prior to widespread mineralization. Although pumping tests show that the hydraulic conductivity of CRBG entablatures is approximately seven orders of magnitude lower than the composite injection zone, the permeability of these units is governed primarily by fracture networks. This means that permeability in the flow interiors may be highly sensitive to fracture dilation because permeability is known to scale nonlinearly with aperture.[52] A typical estimate for the onset of fracture dilation is when fluid pressure exceeds the normal stress acting on a fault plane[51]; however, the concept of a 'deformable fracture' has been shown

relevant for quantifying aperture changes in response to changing effective normal stress on a fracture plane.[12,53–55] To quantify the deformable nature of a fracture, the specific stiffness (κ) is invoked, such that κ is the ratio of change in effective normal stress ($\Delta\sigma_{n,eff}$) to change in fracture aperture (Δe). In crystalline rocks, experimental results show that κ is $\sim$100 MPa mm^{-1} for effective normal stress conditions expected at the Wallula site.[53] Since stress-dependent permeability is highly nonlinear, particularly below 5 MPa effective stress, we implement a conservative fracture dilation criterion of $\sigma_{n,eff} \leq 5$ MPa, which in the entablature overlying the proposed injection zone correlates with ΔP_f of $\sim$5 MPa and > 0.1 mm fracture dilation.

At the Wallula site, the smallest effective normal stress that can act on fault plane is the minimum compressive effective stress $S_{V,eff}$, suggesting that column-normal (horizontal) fractures in the $S_H - S_h$ plane may be the first to dilate in the presence of excessive fluid pressure. To compute the potential for fracture dilation within the sealing formation (entablature) overlying the injection zone (Fig. 2), the dilation criterion of $S_{V,eff} \leq 5$ MPa is evaluated within each grid cell of the ensemble. To assess the potential for >1% dilation within the Wallula sealing formations, this criterion was augmented to account for uncertainty in the fluid pressure component of $S_{V,eff}$:

$$S_V - [\bar{P}_{f(x,y,z)}(t) + 3s_{(x,y,z)}] \leq 5\text{MPa} \qquad (7)$$

where, $s_{(x,y,z)}$ is the standard deviation of $\bar{P}_{f(x,y,z)}(t)$ at time t.

At the borehole scale, tensile failure (hydraulic fracture) is governed by the interactions between radial stress concentrations along the borehole wall, well bore fluid pressure, and the far-field horizontal stresses, S_H and S_h. Horizontal compressive stresses acting normal to the borehole circumference are deflected 90° as tensile stresses, whereas horizontal compressive stresses acting tangential to the borehole will be magnified 3×. These local scale effects become superimposed on the regional stress field, which results in a somewhat complex criterion for hydraulic fracture (or breakdown) pressure (P_b):

$$P_b = \frac{3S_h - S_H + T_o - 2\eta P_f}{1 + \beta - 2\eta} \qquad (8)$$

$$\eta = \frac{\alpha(1 - 2\nu)}{2(1 - \nu)} \qquad (9)$$

$$\alpha = 1 - \frac{\beta_i}{\beta_b} \tag{10}$$

where T_o is the tensile strength of rock, β is the effective stress coefficient for tensile failure, and η accounts for poroelastic effects in a permeable rock mass.[56] This poroelastic term includes the bulk and unfractured rock mass compressibility (β_b and β_i, respectively), Poisson's ratio (ν) and the Biot parameter (α) all of which have been constrained for either CRBG basalts[57–59] or analogous jointed basalt formations.[60,61] To assess the potential for fluid pressure in excess of P_b during the CCS scenario presented here at the Wallula Site, Eqn (8) is solved for each grid cell representing the CO$_2$ injection zone.

At the reservoir scale, that is, far-field from the CO$_2$ injection well, the potential for tensile failure is governed primarily by the regional stress field, microcrack geometry, intact rock properties, and pore fluid pressure.[51] The tensile failure criterion for a poroelastic rock mass is the fluid pressure above which new joints can be formed, that is, the joint initiation pressure (P_i):

$$P_i = \frac{K_{IC}}{Y\sqrt{c}} + \frac{\nu}{1-\nu}S_V + \frac{(1-2\nu)}{(1-\nu)}\alpha P_f \tag{11}$$

where K_{IC} is the fracture toughness, Y is the crack-shape factor, and c is the crack half-length.[51] In this formulation for joint initiation pressure, K_{IC} is used in place of uniaxial tensile strength because K_{IC} accounts for the shape and size of cracks, which, in combination with the crack-shape factor (Y), is more representative of the unfractured rock mass.[51] Constraints on K_{IC} are provided in DeGraff and Aydin.[58] In applying the crack-shape factor Y, the two choices suggested by Sih[62] are accounted for: $Y = \frac{2}{\sqrt{\pi}}$ for a penny-shaped initial crack, and $Y = \sqrt{\pi}$ for a blade-shaped initial crack. Microcrack geometry in basalt rocks generally occurs along individual grain boundaries, so that microcrack length is limited by grain size, for example, the average observable crack lengths in Icelandic basalt is ∼0.01 mm on the basis of scanning electron microscope (SEM) imaging.[63] To assess the potential for fluid pressure in excess of P_i during the CCS scenario considered here, Eqn (11) is solved for each grid cell in the domain with a particular interest in the composite injection zone between 775 and 865 m below ground surface. Here, the P$_f$ term in Eqn (11) is replaced with mean simulated pore fluid pressure for selected time steps ($\bar{P}_{f(inj)}$), and the

likelihood of <1% tensile failure is assessed by increasing $\bar{P}_{f(inj)}$ by three standard deviations.

Results and discussion

This study implements ensemble simulation methods to test the feasibility of industrial-scale CCS in a flood basalt reservoir with characteristics of the Wallula Basalt Sequestration Pilot Project in southeast Washington State (USA). To account for highly uncertain and *a priori* unknowable permeability distributions beyond the well bore, the model scenario is simulated within 35 synthetic reservoirs comprising equally probable and spatially correlated permeability distributions. Ensemble analytics (e-type estimates) are used to bound the uncertainty of both injection-induced pressure transients and CO$_2$ saturation. These results are combined with threshold criteria for geomechanical reservoir performance in composite injection zone and overlying flow interiors (sealing units). The following section includes results and discussion for shear failure (Eqns (5) and (6)), fracture dilation (Eqn (7)), borehole breakout (Eqns (8–(10)), and joint-initiation pressure (Eqn (11)).

Spatial variability

The Columbia River Basalt Group exhibits highly heterogeneous and spatially correlated permeability, which imposes considerable influence on both CO$_2$ plume geometry and injection-induced fluid pressure accumulation. These effects are most pronounced within the uppermost portion of the composite injection zone, where the ensemble mean calculations (Eqn (1)) show that (i) free-phase CO$_2$ at 1% saturation extends radially ∼425 m from the injection well after 1 year and (ii) maximum injection pressure reaches ∼24.5 MPa (Fig. 6). The temporal evolution of both fluid overpressure (Fig. 6, red contour line) and 1% CO$_2$ saturation (Fig. 6, black contour line) indicate that fluid pressure propagates much faster than CO$_2$ transport and in different spatial configurations. Within the first month of injection, the CO$_2$ has migrated 20 m, while the reservoir experiences increased fluid pressures up to 1000 m away. Across the complete ensemble, the bulk pressure front radiates in an elliptical pattern (Fig. 6). The long axis of this ellipse is oriented ∼N40°E, which is the direction of maximum spatial correlation for CRBG permeability.[36] This indicates that the spatial correlated permeability is
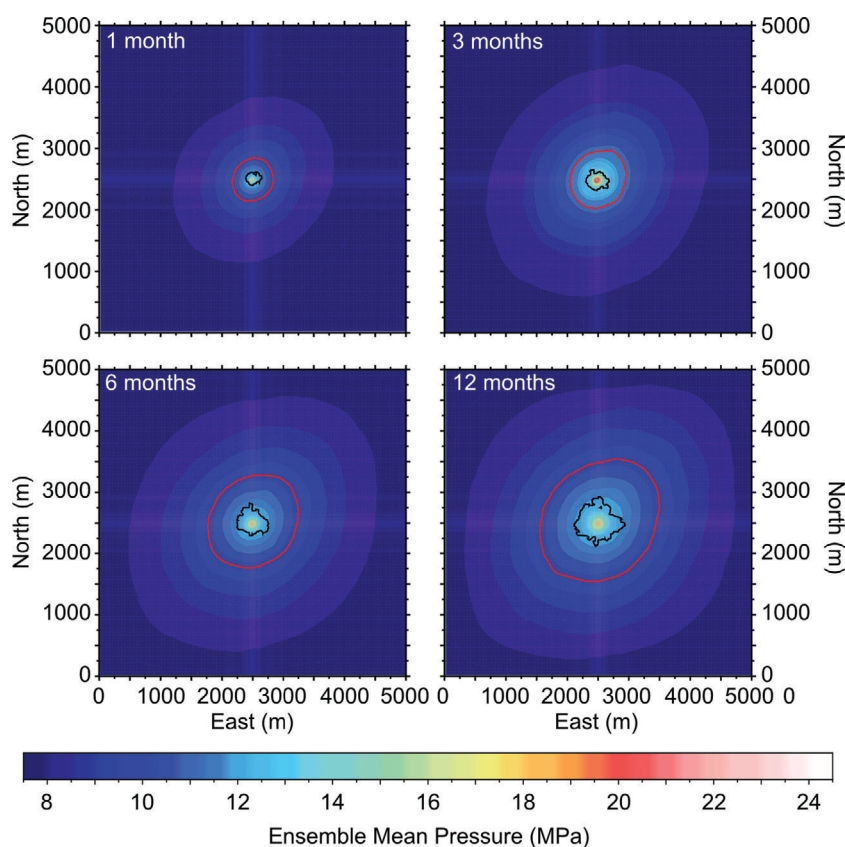
Figure 6. Ensemble mean fluid pressure ($N = 35$) (Eqn (1)) within the uppermost injection interval (775–780 m depth) at time steps ranging from 1 to 12 months. Black contour line denotes 0.01 (1%) CO₂ saturation. Area within red contour line denotes fluid pressure $\geq$2.5 MPa above preinjection levels.

a first-order control over the ensemble mean pressure distribution within the model.

The different geometric configurations assumed by the injection-induced pressure front and the CO₂ plume are most likely explained by the different mechanisms governing saturated and unsaturated flow. For example, Pollyea *et al.*[18] showed that relative permeability feedbacks exacerbate the influence of highly conductive flow paths because free-phase CO₂ will initially enter a high permeability flow path, and in doing so the nonwetting phase (CO₂) permeability increases thus increasing conductivity of the initial flow path and further increasing CO₂ mobility. In addition, Pollyea[28] showed that fluid pressure propagation is largely controlled by wetting phase drainage, thus far-field pressure transients are governed by fully saturated permeability. As a consequence, CO₂ migration is concentrated in the most conductive, near-field flow paths as nonwetting phase permeability

increases, while far-field pressure diffusion is governed by the larger scale bulk permeability architecture.

The uncertainty implied by the ensemble calculations is further reinforced in the context of individual realizations. For example, Fig. 7 shows the change in pressure and free-phase CO₂ saturation for an individual simulation run after 1 year of injection. In this simulation run, fluid pressure propagates asymmetrically to the southeast across the full thickness of the disposal reservoir. In contrast, the CO₂ plume trends north-south at the top of the reservoir, while minimal CO₂ has accumulated deeper within the reservoir. This result shows that the combination of buoyancy forces,[64] relative permeability feedbacks,[18,22] and reservoir heterogeneity[19] work in aggregate to control the CO₂ plume geometry. The overall implication of these results suggest that fluid pressure monitoring is unlikely to be an effective predictor of CO₂ plume geometry or breakthrough; however, recent
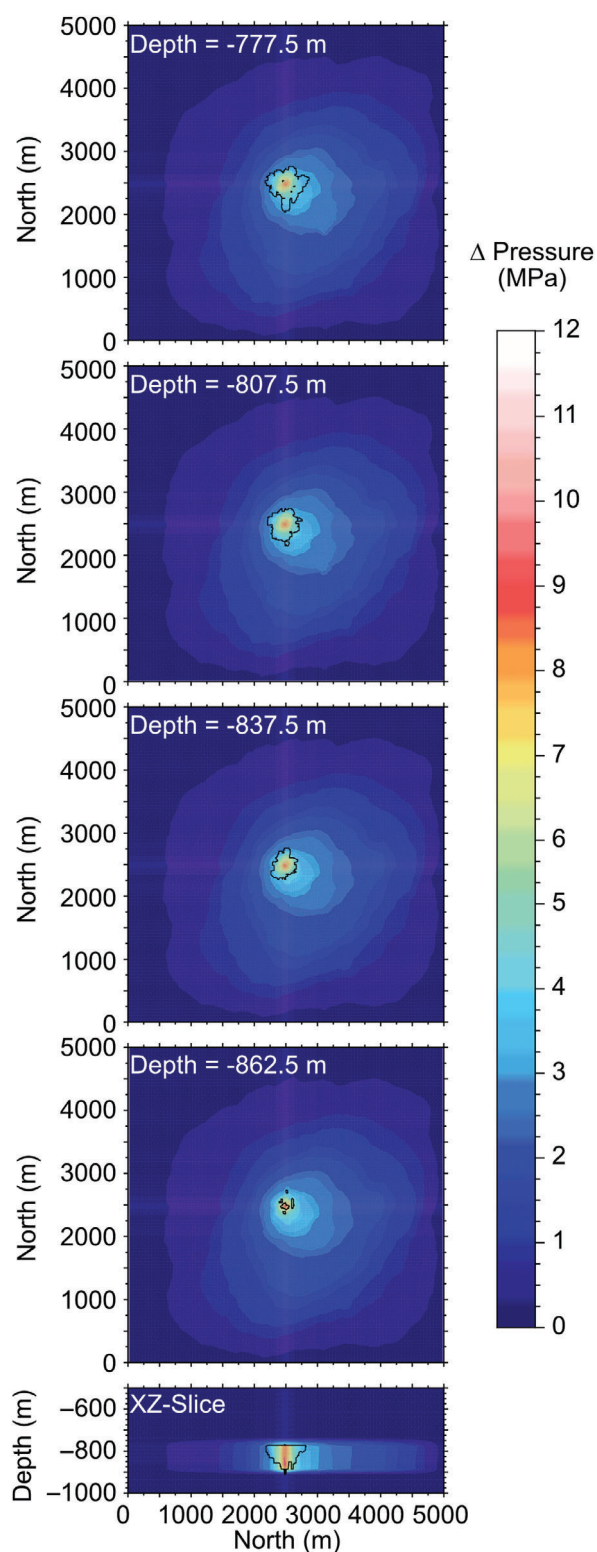
Figure 7. Injection-induced fluid pressure change (ΔP_f) for a single realization after 10 years of injection. Top four panels are horizontal slices and the bottom panel is an *xz*-slice through the injection well. Black contour line denotes 1% free-phase CO₂ saturation.

Potential for injection-induced shear failure

Fluid pressure transients caused by industrial-scale CCS operations may drive effective stress below the stable stress envelope (Fig. 5) inducing slip on optimally aligned faults or fractures. This consideration is particularly relevant for CCS in basalt formations because they are characterized by fanning columnar joints (Fig. 2), of which a subset is likely to optimally align with the regional stress field. This is further complicated because the orientation of basalt fracture networks at depths of interest for CCS are *a priori* unknowable at spatial scales beyond the borehole(s). To arrive at a conservative (worst case) estimate of the potential for injection-induced shear failure, the Mohr–Coulomb failure criterion is evaluated at each grid cell in the model domain using Eqn (4), but modified to account for effective stress. Within the model scenario considered here, shear failure is probable for any optimally oriented fractures within 2000 m of the injection well after 1 year of injection (Fig. 8, black contour) and the bounding entablature layer (Fig. 9, black contour). The uncertainty about this result is calculated for three standard deviations variation about the mean (Figs 8 and 9, orange contour), which illustrates reservoir volume within which the probability of inducing shear failure in the target reservoir is greater than 1%.

These results suggest that a shear failure may occur on optimally aligned fractures within a substantial volume of the target reservoir. Because the CRBG is relatively aseismic, these results suggest that numerous cm-scale displacements are more likely to affect storage potential and seal efficacy than large-scale displacements that are known to trigger earthquakes during oilfield wastewater disposal.[66] The implications of numerous cm-scale displacements are that shear dilation may increase fracture permeability resulting in hydraulic pathways for the CO₂ to escape the disposal reservoir.[14] The entablature layers shown in Fig. 9 represents the caprock seal separating the current injection zone from another high permeability zone above it (~750 m depth, Fig. 2). This suggests that shear failure may occur optimally aligned fractures within a substantial volume of the caprock, which may

research suggests that the thermal signature from CO₂ dissolution may be an effective tool for breakthrough monitoring.[65]
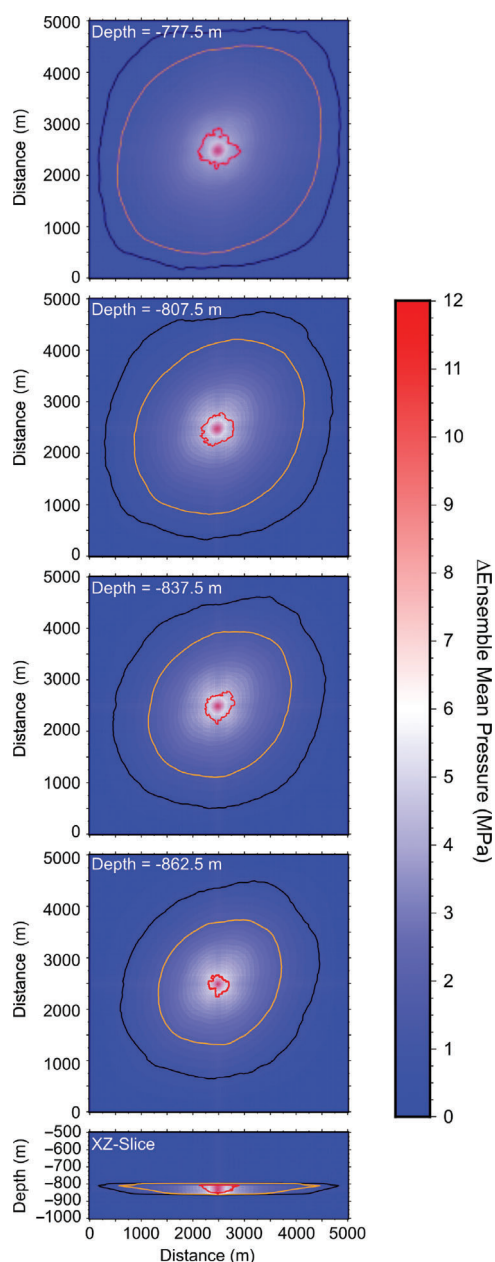
Figure 8. Potential for shear failure after 1 year of injection in four horizontal slices through the composite injection zone (top four panels) and one vertical slice through the injection well (bottom panel). Each panel is colored by ensemble mean fluid pressure change ($\Delta \bar{P}_f$). Area within black contour exceeds Mohr–Coulomb failure criterion when minimum effective stress is calculated on the basis of ensemble mean fluid pressure. Area within orange contour comprises $\geq 1\%$ probability of shear failure calculated by Eqn 6. Area within red contour line is $\geq 1\%$ free-phase CO₂ saturation.
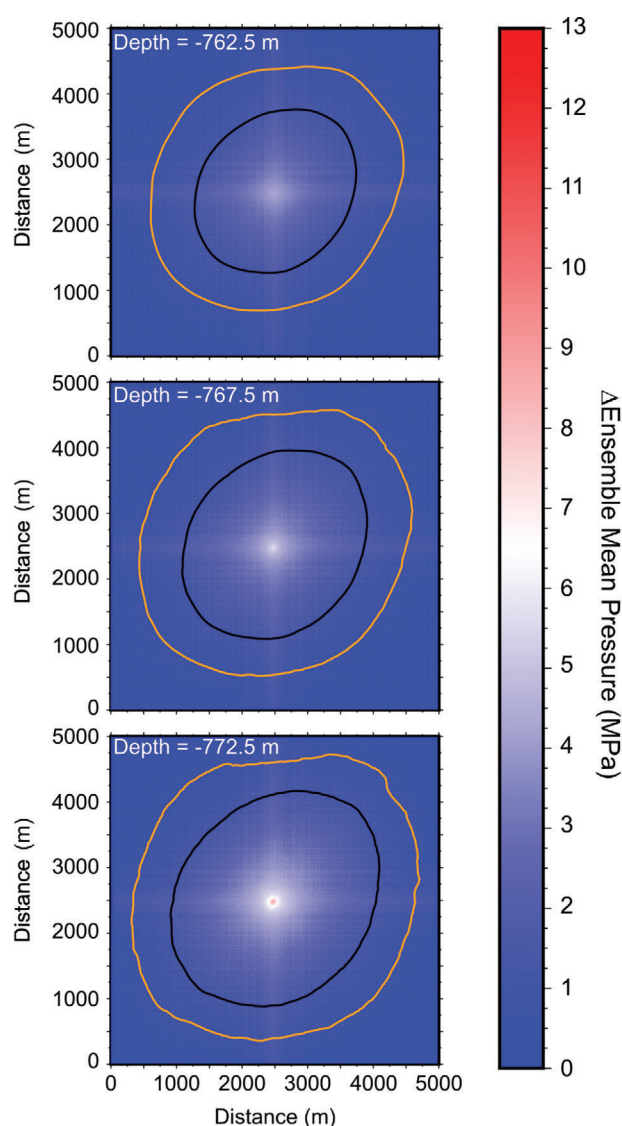

Figure 9. Potential for shear failure after 1 year of injection in three horizontal slices through the entablature layer bounding the injection zone. Each panel is colored by ensemble mean fluid pressure change ($\Delta \bar{P}_f$). Area within black contour exceeds Mohr–Coulomb failure criterion when minimum effective stress is calculated on the basis of ensemble mean fluid pressure. Area within orange contour comprises $\geq 1\%$ probability of shear failure calculated by Eqn 6.

facilitate leakage out of the storage reservoir. However, the CO₂ sequestration in basalt reservoirs is predicated on rapid conversion of CO₂ into permanent mineral phases, the result of which decreases permeability as fractures are filled with secondary alteration products.[67] As a result, basalt fracture networks may exhibit self-sealing characteristics, which would offset

the adverse effects of permeability enhancement caused by cm-scale displacements on optimally oriented fractures. However, further research is clearly warranted to gain a more complete understanding of the complex feedbacks between hydraulic, chemical, and mechanical processes.

Fracture dilation in overlying flow interior

During industrial-scale CO$_2$ injections, pressure transients may propagate beyond the disposal reservoir into the overlying flow interior that serves as a caprock seal prior to widespread mineralization. Although basalt flow interiors are characterized by substantially lower permeability (up to 7 orders of magnitude) than the injection interval, this pressure propagation may dilate pre-existing fractures leading to reservoir leakage. To quantify the potential for fracture dilation to affect the flow interior overlying the composite injection zone in this study, the probability of 1% fracture dilation is calculated for three standard deviations above the ensemble mean fluid pressure (Eqn (7)). Figure 10 presents the results of this calculation in comparison with the ensemble mean fluid pressure change ($\Delta \bar{P}_f$) after 1, 3, 6, and 12 months of injection. These results show that the probability of fracture dilation exceeds 1% within ~1000 m radial distance of the injection well after 1 year.

These results are congruent with a number of studies that show pressure transients induced by CO$_2$ injection operations affect a much larger reservoir volume than the fluid itself.[68–70] This is apparent in Fig. 7, which shows that the injected CO$_2$ migrates a maximum of 400 m, while the target reservoir experiences pressure changes up to 2200 m away from the injection well. Similarly, Birkholzer *et al.*[71] show that after a 30 year CO$_2$ injection from a single well, a pressure increase of 100 kPa extends almost 85 km laterally, while the CO$_2$ only migrates ~2 km. In the context of vertical CO$_2$ flow, the simulation results presented here show that no free-phase CO$_2$ enters the overlying flow interior; however, this may be an artifact of the static permeability approach, that is, permeability in the model does not vary with changes in effective stress. Nevertheless, this result agrees with the outcrop-scale study by Gierzynski and Pollyea[21], which shows that free-phase CO$_2$ only migrates upwards ~3 m over 10 years when entering from below at constant overpressure. These authors show that relative permeability causes free-phase CO$_2$ to accumulate at
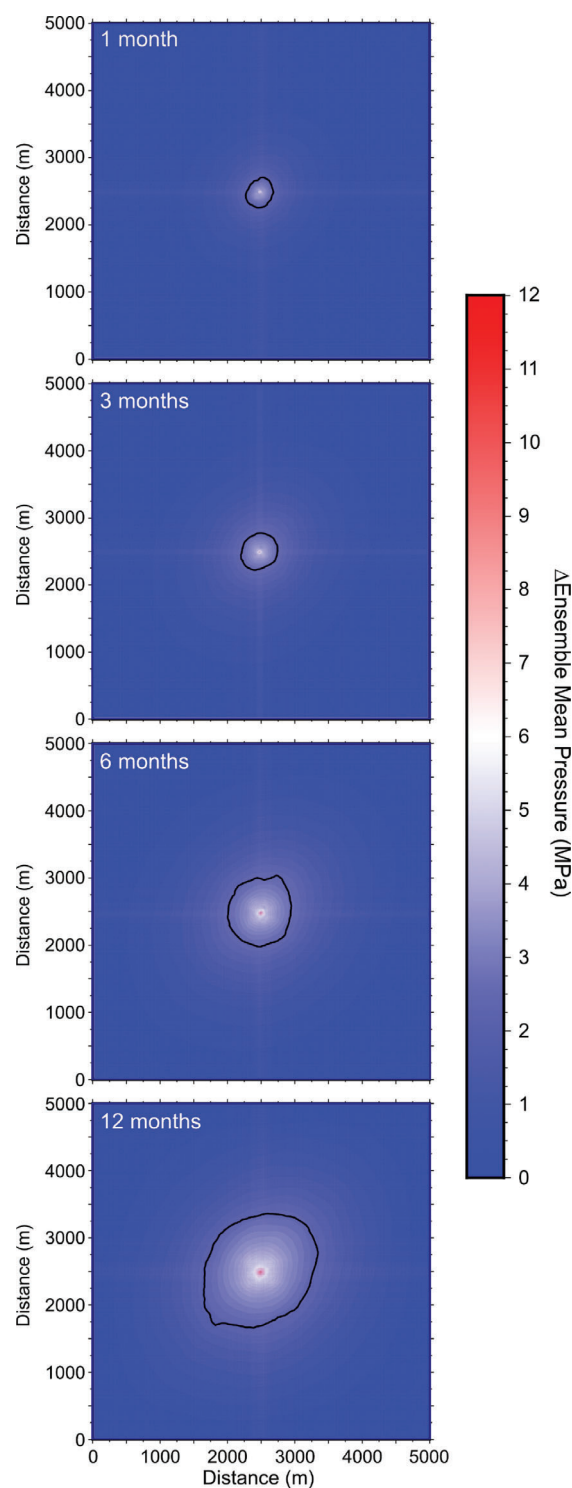

Figure 10. Potential for fracture dilation the basalt flow interior that overlies the composite injection zone (770–775 m depth) after 1, 3, 6, and 12 months. Each panel is colored by ensemble mean fluid pressure change ($\Delta \bar{P}_f$). Area inside black contour lines denotes $\geq 1\%$ probability that preexisting fractures will experience dilation.
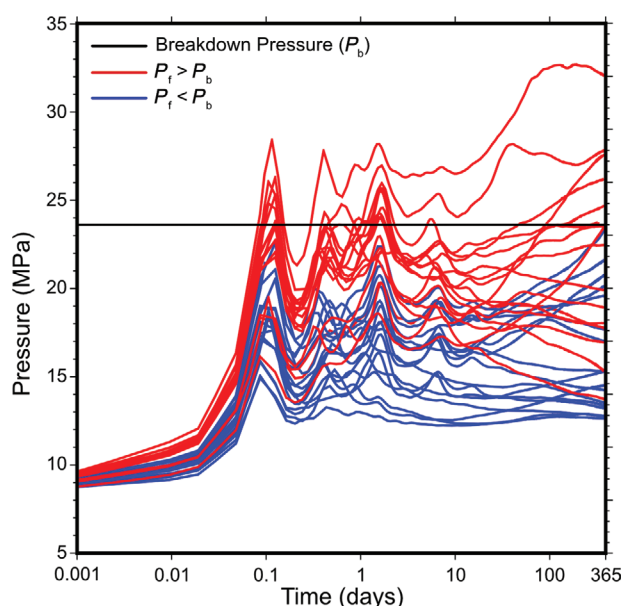
 |

Figure 11. Time series of injection pressure for each simulation in the ensemble. The black line indicates the pressure above which borehole break will occur (P$_b$). Red lines denote simulation results that exceed breakdown pressure within the 1 year injection period. Blue lines denote simulation results that remain below breakdown pressure for the injection period. Half (50%) of the simulations exceed P$_b$.

fracture intersections, thus slowing the leakage rate. Similarly, Jayne *et al.*[23] simulate CO$_2$ injections into a flood basalt reservoir at constant pressure and shows that free-phase CO$_2$ only migrates 25 m into the entablature after 20 years of CO$_2$ injection. Although these former results are generally encouraging, additional advances in stress-dependent permeability are needed to more fully understand this process.

Borehole breakdown

The time series of injection pressure is shown in Fig. 11 for each of the 35 simulations. Because the model scenario delivers CO$_2$ at a constant mass flow rate, variations of fluid pressure are due solely to the spatially variable and equally probable permeability distributions. Results show that maximum injection pressure ranges from ~14.5 to 34 MPa (hydrostatic pressure = 8.5 MPa), which results in 50% of the simulations exceeding the borehole breakdown threshold of 23.7 MPa (Eqn (8)). For simulations exceeding the breakdown criterion (Fig. 11, red lines), fluid pressure rapidly increases and the threshold is exceeded within 1 day of injection. However, injection

pressure in several simulations remains below the breakdown threshold for several months before exceeding the breakdown threshold. Research by Pollyea[28] shows the pressure accumulation during CO$_2$ injections is controlled primarily by wetting-phase relative permeability. Because the relative permeability characteristics of basalt reservoirs are highly interfering,[48] a small increase in CO$_2$ saturation results in a large drop in wetting-phase permeability. As a result, injection pressure accumulation is strongly influenced by the interconnectedness of high permeability flow paths away from the borehole.[18] And while it is unlikely that an industrial-scale CCS project will operate at constant mass flow rates for 12 months, the broader implication is of these results is that permeability variability in the near field strong influences overall reservoir injectivity.

Joint initiation

In basalt reservoirs, the initiation and propagation of new fractures presents an operational paradox that remains unresolved. Specifically, fracture initiation and propagation may facilitate reservoir leakage before widespread mineralization can isolate the CO$_2$. However, new fractures also provide fresh surface area, which increases the mineral storage potential of the reservoir. Although this study does not purport to answer this underlying research question, we begin to understand its scope by constraining the spatial extent for which the probability of new joint initiation is ≥1%. Figure 12 presents the volume within which the probability of joint initiation is ≥1% after 1, 3, 6, and 12 months (Eqn (11)). These results show that the probability of joint initiation ≥1% occurs within ~75 m from the well after 3 months, and increases to 125 m after 1 year. This indicates that joint initiation primarily occurs within areas of the reservoir occupied by free-phase CO$_2$, and, as a result, joint initiation will increase leakage potential. This result contrasts with the spatial extent of shear failure ≥1% (Fig. 8), which encompasses a much larger footprint than the CO$_2$ plume. For example, probability of joint initiation ≥1% is likely to occur within 125 m of the injection well after 1 year, whereas the corresponding probability of shear failure extends beyond 2300 m away from the injection well.

Joint initiation is the process of generating tensile fractures, which open in the direction of the least compressive principle stress, and then propagate in the
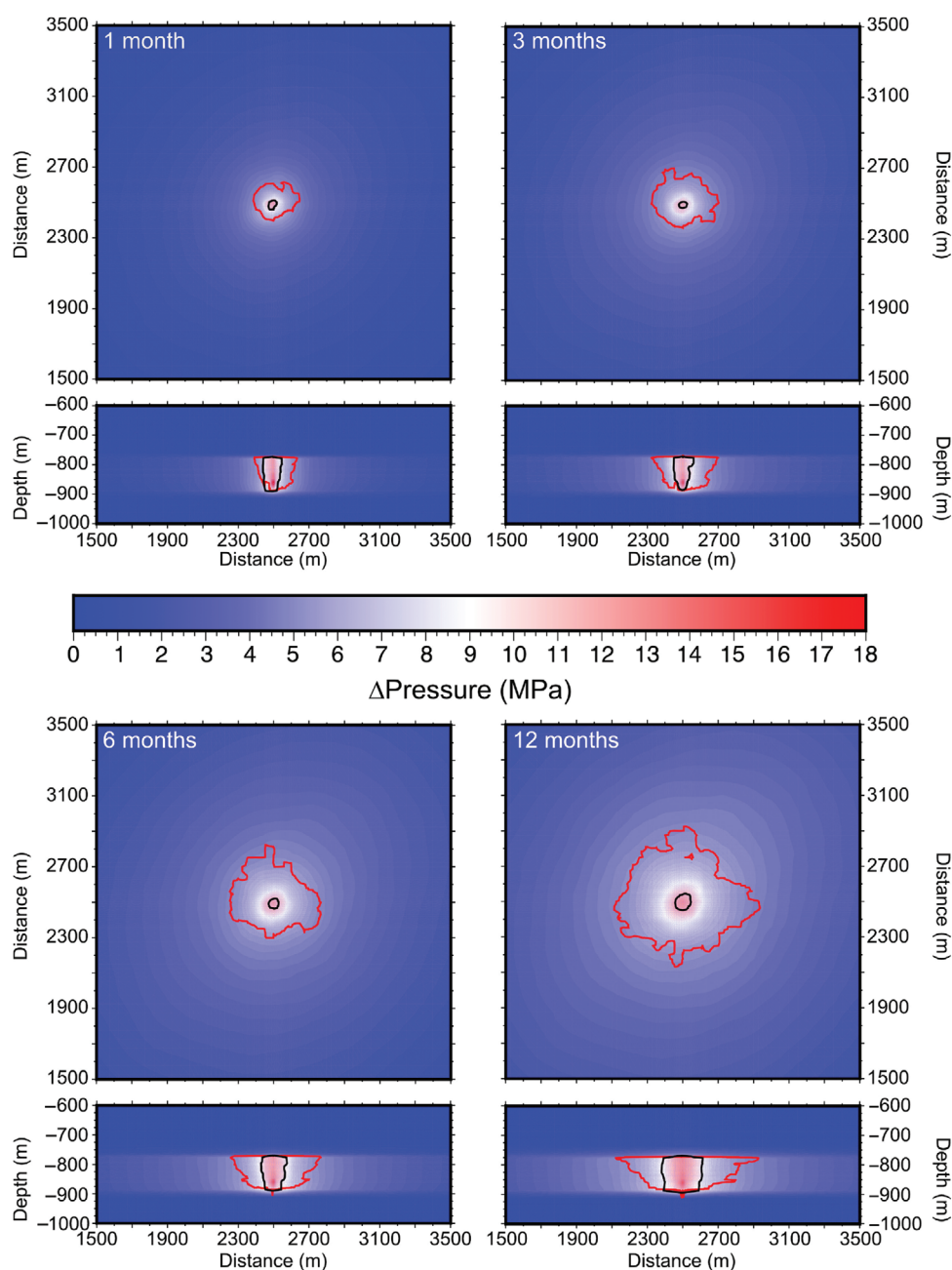
Figure 12. Potential for joint initiation within the uppermost layer of the composite injection zone (775–780 m depth) after 1, 3, 6, and 12 months of injection. Each panel is a horizontal and vertical slice and note time. Shading denotes ensemble mean fluid pressure ($\Delta \bar{P}_f$). Area within black contours denotes $\geq 1\%$ probability of joint initiation. Red contours represent 1% CO$_2$ saturation.

plane of the intermediate and greatest compressive principle stresses. Because the Columbia River Plateau is in a compressive stress regime (σ_3 is vertical), new fractures will open in the vertical direction and propagate horizontally. Although this is a favorable scenario for CO$_2$ storage, basalt formations are characterized by columnar (vertical) joints, and, as a result, joint initiation is likely to increase the connectivity of fracture networks. This may be a positive outcome in the context of overall reservoir injectivity because this study finds that borehole breakdown is largely controlled by the interconnected

|

fracture networks within close proximity to the borehole, where the probability of joint initiation is highest.

Conclusions

Flood basalts have been gaining recognition as potential reservoirs for carbon capture and sequestration. The success of recent field experiments in Washington State (USA) and Iceland shows that injected CO$_2$ will interact with the basalt to form carbonate minerals at the field scale and very short timescales. However, upscaling these field-scale experiments to industrial-scale CO$_2$ injections is required if CCS is going to be an effective strategy to mitigate climate change. Transitioning basalt CCS from the pilot scale to industrial scales introduces a number of uncertainties, including feedbacks between multiphase flow processes and fracture-controlled reservoir properties, incomplete knowledge of reservoir characteristics, and coupled dynamics between hydraulic, thermal, mechanical, and geochemical processes. This study is an important first step toward understanding the relationships between multiphase fluid flow processes, spatial reservoir uncertainty, and reservoir geomechanics. We implement ensemble simulation and analytics to bound the uncertainty associated with industrial-scale CO$_2$ injection into a flood basalt reservoir. For a single CO$_2$ injection well operating at a constant mass injection of 21.6 kg/s, we find the following points:

1. The aggregate behavior over the ensemble of simulations shows that fluid pressure forms roughly an ellipse around the injection well trending N40°E, which suggests that the permeability correlation structure exhibits control on the pressure evolution within the target reservoir.
2. Joint initiation mainly occurs around or within the CO$_2$ plume during the injection phase. Joint initiation within the injection may increase permeability leading to better injectivity and storage, but if these joints coalesce into a larger fracture network it may compromise the integrity of the reservoir.
3. Fluid pressure builds rapidly during a CO$_2$ injection causing the storage reservoir to experience increased fluid pressures up to 1000 m away within the first month and 2200 m away during the first year.

4. Results from this study suggest that implementing multiple injection wells to accommodate the annual CO$_2$ emission from a 500 MW power plant may be an effective strategy to mitigate the potential for geomechanical reservoir failure. The effects of multiple wells may effectively offset the uncertainty that is presented by highly heterogeneous permeability fields in the mid- to far-field regions.
5. Combining ensemble simulation with geomechanical threshold criteria is an effective method for risk analysis associated with a CCS project.

In conclusion, these results suggest that the implementation of a regional data set and spatial correlation structures into a numerical model can provide insights into the behavior of fluid pressure within heterogeneous reservoirs. Additionally, these results illustrate the uncertainty associated with highly heterogeneous flood basalt reservoirs and a CCS project would require extensive reservoir characterization for a geomechanical risk assessment. Significantly more research is required to develop a better understanding of the reactive transport, thermal processes, fracture behavior, and response associated with an industrial-scale CO$_2$ injection into a flood basalt reservoir.

Acknowledgements

References

1. McGrail BP, Schaef HT, Ho AM, Chien YJ, Dooley JJ and Davidson CL, Potential for carbon dioxide sequestration in flood basalts. *J Geophys Res* **111**(B12) (2006). https://doi.org/10.1029/2005JB004169
2. Matter JM and Kelemen PB, Permanent storage of carbon dioxide in geological reservoirs by mineral carbonation. *Nat Geosci* **2**(12):837–841 (2009).
3. Matter JM, Stute M, Snæbjörnsdottir SÓ, Oelkers EH, Gislason SR, Aradottir ES *et al.*, Rapid carbon mineralization for permanent disposal of anthropogenic carbon dioxide emissions. *Science* **352**(6291):1312–1314 (2016).

4. McGrail BP, Schaef HT, Spane FA, Cliff JB, Qafoku O, Horner JA *et al.*, Field validation of supercritical CO$_2$ reactivity with basalts. *Environ Sci Technol Lett* **4**(1):6–10 (2017).

5. Goldberg DS, Takahashi T and Slagle AL, Carbon dioxide sequestration in deep-sea basalt. *Proc Natl Acad Sci USA* **105**(29):9920–9925 (2008).

6. Goldberg DS, Kent DV and Olsen PE, Potential on-shore and off-shore reservoirs for CO$_2$ sequestration in Central Atlantic magmatic province basalts. *Proc Natl Acad Sci USA* **107**(4):1327–1332 (2010).

7. Price PN and Oldenburg CM, The consequences of failure should be considered in siting geologic carbon sequestration projects. *Int J Greenh Gas Control* **3**(5):658–663 (2009).

8. USDOE, Carbon technology program plan. United States Department of Energy, Washington, D.C. (2013).

9. Shaffer G, Long-term effectiveness and consequences of carbon dioxide sequestration. *Nat Geosci* **3**(7):464 (2010).

10. Lucier A, Zoback M, Gupta N and Ramakrishnan T, Geomechanical aspects of CO$_2$ sequestration in a deep saline reservoir in the Ohio River Valley region. *Environ Geosci* **13**(2):85–103 (2006).

11. Goodarzi S, Settari A, Zoback M and Keith D, A coupled geomechanical reservoir simulation analysis of carbon dioxide storage in a saline aquifer in the Ohio River Valley. *Environ Geosci* **18**(3):189–207 (2011).

12. Min KB, Rutqvist J, Tsang CF and Jing L, Stress-dependent permeability of fractured rock masses: A numerical study. *Int J Rock Mech Min Sci* **41**(7):1191–1210 (2004).

13. Cappa F and Rutqvist J, Impact of CO$_2$ geological sequestration on the nucleation of earthquakes. *Geophys Res Lett* **38**(17) (2011). https://doi.org/10.1029/2011GL048487

14. Zoback MD and Gorelick SM, Earthquake triggering and large-scale geologic storage of carbon dioxide. *Proc Natl Acad Sci USA* **109**(26):10164–10168 (2012).

15. NETL, *Best Practices for: Risk Analysis and Simulation of Geologic Storage of CO$_2$*. NETL, Washington, DC (2011).

16. Srivastava RM, An overview of stochastic methods for reservoir characterization. *AAPG Comput Appl Geol* **3**:3–16 (1994).

17. Li Y, LeBoeuf EJ, Basu PK and Mahadevan S, Stochastic modeling of the permeability of randomly generated porous media. *Adv Water Resour* **28**(8):835–844 (2005).

18. Pollyea RM and Fairley JP, Implications of spatial reservoir uncertainty for CO$_2$ sequestration in the east Snake River Plain, Idaho (USA). *Hydrogeol J* **20**(4):689–699 (2012).

19. Pollyea RM, Fairley JP, Podgorney RK and Mcling TL, Physical constraints on geologic CO$_2$ sequestration in low-volume basalt formations. *Geol Soc Am Bull* **126**(3-4):344–351 (2014).

20. Popova OH, Small MJ, McCoy ST, Thomas A, Rose S, Karimi B *et al.*, Spatial stochastic modeling of sedimentary formations to assess CO$_2$ storage potential. *Environ Sci Technol* **48**(11):6247–6255 (2014).

21. Gierzynski AO and Pollyea RM, Three-phase CO$_2$ flow in a basalt fracture network. *Water Resour Res* **53**(11):8980–8998 (2017).

22. Jayne R, Hao W and Pollyea R, Geologic CO$_2$ sequestration in a basalt reservoir: Constraining permeability uncertainty within the Columbia River Basalt Group. *TOUGH Symposium*, Lawrence Berkeley National Laboratory, Berkeley, CA (2018).

23. Jayne RS, Wu H and Pollyea RM, Geologic CO$_2$ sequestration and permeability uncertainty in a highly heterogeneous reservoir. *Int J Greenh Gas Control* **83**:128–139 (2019).

24. Bosshart NW, Azzolina NA, Ayash SC, Peck WD, Gorecki CD, Ge J *et al.*, Quantifying the effects of depositional environment on deep saline formation CO$_2$ storage efficiency and rate. *Int J Greenh Gas Control* **69**:8–19 (2018).

25. Tidwell VC and Wilson JL, Laboratory method for investigating permeability upscaling. *Water Resour Res* **33**(7):1607–1616 (1997).

26. Saar M and Manga M, Depth dependence of permeability in the Oregon Cascades inferred from hydrogeologic, thermal, seismic, and magmatic modeling constraints. *J Geophys Res* **109** (B4) (2004). https://doi.org/10.1029/2003JB002855.

27. Mathias SA, Gluyas JG, González Martínez de Miguel GJ and Hosseini SA, Role of partial miscibility on pressure buildup due to constant rate injection of CO$_2$ into closed and open brine aquifers. *Water Resour Res* **47**(12) (2011). https://doi.org/10.1029/2011WR011051.

28. Pollyea RM, Influence of relative permeability on injection pressure and plume configuration during CO$_2$ injections in a mafic reservoir. *Int J Greenh Gas Control* **46**:7–17 (2016).

29. Reidel SP, Spane FA and Johnson VG, Natural gas storage in basalt aquifers of the Columbia basin, Pacific Northwest USA: A guide to site characterization. Pacific Northwest National Laboratory (PNNL), Richland, WA (2002).

30. McGrail B, Sullivan E, Spane F, Bacon D, Hund G, Thorne P *et al.*, Topical report–preliminary hydrogeologic characterization results from the Wallula Basalt Pilot Study. Technical report, Report PNWD-4129. *Pacific Northwest National Laboratory*, Richland, WA (2009).

31. Burns ER, Morgan DS, Peavler RS and Kahle SC, Three-dimensional model of the geologic framework for the Columbia Plateau Regional Aquifer System, Idaho, Oregon, and Washington. US Geological Survey, Reston, VA (2011).

32. Kahle S, Morgan D, Welch W, Ely D, Hinkle S, Vaccaro J *et al.*, Hydrogeologic framework and hydrologic budget components of the Columbia Plateau Regional Aquifer System, Washington, Oregon, and Idaho. US Geological Survey, Reston, VA (2011).

33. Gephart R, Price S, Jackson R and Myers C, Geohydrologic factors and current concepts relevant to characterization of a potential nuclear waste repository site in Columbia River Basalt, Hanford Stte, Washington, *MRS Proceedings*, vol. 26. Cambridge University Press, Cambridge (1983).

34. Burns ER, Williams CF, Tolan T and Kaven JO, Are the Columbia River Basalts, Columbia Plateau, Idaho, Oregon, and Washington, USA, a viable geothermal target? A preliminary analysis. Proceedings of the 41st Workshop on Geothermal Reservoir Engineering, Stanford, CA (2016).

35. Mangan MT, Wright TL, Swanson DA, and Byerly GR, Regional correlation of Grande Ronde Basalt flows, Columbia River Basalt Group, Washington, Oregon, and Idaho. *Geol Soc Am Bull* **97**(11):1300–1318 (1986).

36. Jayne RS and Pollyea RM, Permeability correlation structure of the Columbia River Plateau and implications for fluid system architecture in continental large igneous provinces. *Geology* **46**(8):715–718 (2018).

37. Litynski JT, Klara SM, McIlvried HG and Srivastava RD, The United States Department of Energy's regional carbon sequestration partnerships program: A collaborative approach to carbon management. *Environ Int* **32**(1):128–144 (2006).

  |

38. Rodosta T, Litynski J, Plasynski S, Spangler L, Finley R, Steadman E *et al.*, US Department of Energy's regional carbon sequestration partnership initiative: Update on validation and development phases. *Energy Procedia* **4**:3457–3464 (2011).

39. McGrail B, Spane F, Sullivan E, Bacon D and Hund G, The Wallula basalt sequestration pilot project. *Energy Procedia* **4**:5653–5660 (2011).

40. Deutsch CV, *Geostatistical Reservoir Modeling*. Oxford University Press, New York (2002).

41. Deutsch CV and Journel AG, *GSLIB: Geostatistical Software Library and User's Guide*. Oxford University Press, New York (1998).

42. Haukwa C, *AMESH A Mesh Creating Program for the Integral Finite Difference Method: A User's Manual*. Lawrence Berkeley National Laboratory, Berkeley, CA (1998).

43. Jung Y, Pau GSH, Finsterle S and Pollyea RM, TOUGH₃: A new efficient version of the TOUGH suite of multiphase flow and transport simulators. *Comput Geosci* **108**:2–7 (2017).

44. Pruess K, *ECO₂M: a TOUGH2 Fluid Property Module for Mixtures of Water, NaCl, and CO₂, Including Super-and Sub-critical Conditions, and Phase Change between Liquid and Gaseous CO₂*. Ernest Orlando Lawrence Berkeley National Laboratory, Berkeley, CA (2011).

45. Pollack HN, Hurter SJ and Johnson JR, Heat flow from the Earth's interior: Analysis of the global data set. *Rev Geophys* **31**(3):267–280 (1993).

46. Zakharova NV, Goldberg DS, Sullivan EC, Herron MM and Grau JA, Petrophysical and geochemical properties of Columbia River flood basalt: Implications for carbon sequestration. *Geochem Geophys Geosyst* **13**(11) (2012). https://doi.org/10.1029/2012GC004305.

47. Van Genuchten MT, A closed-form equation for predicting the hydraulic conductivity of unsaturated soils. *Soil Sci Soc Am* **44**:892–898 (1980).

48. Bertels SP, DiCarlo DA and Blunt MJ, Measurement of aperture distribution, capillary pressure, relative permeability, and in situ saturation in a rock fracture using computed tomography scanning. *Water Resour Res* **37**:649–662 (2001).

49. Paillet FL and Kim K, Character and distribution of borehole breakouts and their relationship to in situ stresses in deep Columbia River Basalts. *J Geophys Res* **92**(B7):6223–6234 (1987).

50. Byerlee J, Friction of rocks. in *Rock Friction and Earthquake Prediction*, ed by Byerlee JD, Wyss M. Springer, Berlin, pp. 615–626 (1978).

51. Engelder T, *Stress Regimes in the Lithosphere*, vol. 151. Princeton University Press, Princeton, NJ (2014).

52. Witherspoon PA, Wang JS, Iwai K and Gale JE, Validity of cubic law for fluid flow in a deformable rock fracture. *Water Resour Res* **16**(6):1016–1024 (1980).

53. Pyrak-Nolte L and Morris J, Single fractures under normal stress: The relation between fracture specific stiffness and fluid flow. *Int J Rock Mech Min Sci* **37**(1–2):245–262 (2000).

54. Rutqvist J and Stephansson O, The role of hydromechanical coupling in fractured rock engineering. *Hydrogeol J* **11**(1):7–40 (2003).

55. Jiang XW, Wan L, Wang XS, Liang SH and Hu BX, Estimation of fracture normal stiffness using a transmissivity-depth correlation. *Int J Rock Mech Min Sci* **46**(1):51–58 (2009).

56. Jaeger JC, Cook NG and Zimmerman R, *Fundamentals of Rock Mechanics*. John Wiley & Sons, Hoboken, NJ (2009).

57. Schultz RA, Brittle strength of basaltic rock masses with applications to Venus. *J Geophys Res* **98**(E6):10883–10895 (1993).

58. Degraff JM and Aydin A, Effect of thermal regime on growth increment and spacing of contraction joints in basaltic lava. *J Geophys Res* **98**(B4):6411–6430 (1993).

59. Goehring L and Morris SW, Scaling of columnar joints in basalt. *J Geophys Res* **113**(B10): (2008).

60. Adams L and Gibson R, The compressibilies of dunite and of basalt glass and their bearing on the composition of the earth. *Proc Natl Acad Sci USA* **12** (5):275–283 (1926).

61. Simmons G and Brace WF, Comparison of static and dynamic measurements of compressibility of rocks. *J Geophys Res* **70**(22):5649–5656 (1965).

62. Sih GC, *Handbook of Stress-Intensity Factors: Stress-Intensity Factor Solutions and Formulas for Reference*. Lehigh University, Bethlehem, Pa (1973).

63. Kowallis BJ, Roeloffs EA and Wang HF, Microcrack studies of basalts from the Iceland Research Drilling Project. *J Geophys Res* **87**(B8):6650–6656 (1982).

64. Wu H, Jayne RS and Pollyea RM, A parametric analysis of capillary pressure effects during geologic carbon sequestration in a sandstone reservoir. *Greenh Gases* **8**(6):1039–1052 (2018).

65. Jayne RS, Zhang Y and Pollyea RM, Using heat as a predictor of CO₂ breakthrough in highly heterogeneous reservoirs. *Geophys Res Lett* **46**:5879–5888 (2019).

66. Pollyea RM, Mohammadi N, Taylor JE and Chapman MC, Geospatial analysis of Oklahoma (USA) earthquakes (2011–2016): Quantifying the limits of regional-scale earthquake mitigation measures. *Geology* **46**(3):215–218 (2018).

67. Wu H, Jayne RS and Pollyea RM, Quantifying permeability alteration effects to CO₂ storage potential in a basalt fracture network. Abstract S51F-1615. Fall Meeting of the American Geophysical Union, New Orleans, LA (2018).

68. Van der Meer L, Investigations regarding the storage of carbon dioxide in aquifers in the Netherlands. *Energy Convers Manage* **33**(5-8):611–618 (1992).

69. Holloway S, An overview of the Joule II project the underground disposal of carbon dioxide. *Fuel and Energy Abstracts*, vol. 4 (1996).

70. Gunter W, Bachu S, Law DS, Marwaha V, Drysdale D, MacDonald D *et al.*, Technical and economic feasibility of CO₂ disposal in aquifers within the Alberta Sedimentary Basin, Canada. *Energy Convers Manage* **37**(6–8):1135–1142 (1996).

71. Birkholzer JT, Zhou Q and Tsang CF, Large-scale impact of CO₂ storage in deep saline aquifers: A sensitivity study on pressure response in stratified systems. *Int J Greenh Gas Control* **3** (2):181–194 (2009).

72. Schultz R, Limits on strength and deformation properties of jointed basaltic rock masses. *Rock Mech Rock Eng* **28**(1):1–15 (1995).

Richard S. Jayne

Richard Jayne is currently a PhD candidate at Virginia Polytechnic Institute and State University. His current research utilizes multiphase CO$_2$-bring modeling, stochastic reservoir simulation, and geostatistical analysis to study geologic processes.

Hao Wu

Hao Wu is a PhD candidate in the Department of Geosciences at the Virginia Polytechnic Institute and State University. She has a Master's degree in hydrology and she holds keen interests in the area of computational geological fluid systems, specifically in carbon capture and sequestration.

Ryan M. Pollyea

Dr Ryan M. Pollyea is an assistant professor in the Department of Geosciences at Virginia Tech and Principal Investigator of the Computational Geofluids Lab (www.computationalgeofluids.org). His areas of expertise include multiphase fluid flow in geologic media, numerical modeling, and geostatistical reservoir simulation.